

RSC Advances



This is an *Accepted Manuscript*, which has been through the Royal Society of Chemistry peer review process and has been accepted for publication.

Accepted Manuscripts are published online shortly after acceptance, before technical editing, formatting and proof reading. Using this free service, authors can make their results available to the community, in citable form, before we publish the edited article. This *Accepted Manuscript* will be replaced by the edited, formatted and paginated article as soon as this is available.

You can find more information about *Accepted Manuscripts* in the [Information for Authors](#).

Please note that technical editing may introduce minor changes to the text and/or graphics, which may alter content. The journal's standard [Terms & Conditions](#) and the [Ethical guidelines](#) still apply. In no event shall the Royal Society of Chemistry be held responsible for any errors or omissions in this *Accepted Manuscript* or any consequences arising from the use of any information it contains.

Structural, magnetic and magnetocaloric properties of hexagonal multiferroic $\text{Yb}_{1-x}\text{Sc}_x\text{MnO}_3$ ($x = 0.1$ and 0.2)

Bhumireddi Sattibabu^{1#}, A. K. Bhatnagar^{1,2,*}, K. Vinod³, Awadhesh Mani³, and D. Das¹,

¹*School of Engineering Sciences and Technology, University of Hyderabad, Hyderabad 500046, India*

²*School of physics, University of Hyderabad, Hyderabad 500046, India*

³*Condensed Matter Physics Division, Materials Science Group, IGCAR-Kalpakkam, 603102, India*

^{#,*} *Corresponding authors: bsb.satti@gmail.com and anilb42@gmail.com*

We have studied the effect of Sc doping on structural, magnetic and magnetocaloric properties of multiferroic $\text{Yb}_{1-x}\text{Sc}_x\text{MnO}_3$ ($x = 0.1$ and 0.2). X-ray powder diffraction shows that both samples crystallize in the hexagonal phase with $P6_3cm$ space group. The structural analysis shows decrease in lattice parameter a , decrease in cell volume of the hexagonal unit cell and decrease in the average bond length between Mn-O, with Sc substitution. Magnetic measurements show that the Néel temperature (T_N) increases from 90 K for $x = 0.1$ to 94 K for $x = 0.2$ sample. Isothermal magnetic curves show that the field variation in magnetization generates a metamagnetic transition. The maximum entropy change $-\Delta S_M^{\max}$ and the relative cooling power (RCP) of $\text{Yb}_{1-x}\text{Sc}_x\text{MnO}_3$ are found to be 2.46 ± 0.40 J/mole-K and 38.5 ± 9 J/mol for $x = 0.1$ and 1.87 ± 0.31 J/mole-K and 30.1 ± 8 J/mol for $x = 0.2$ with $\Delta H = 10$ T. The rescaled magnetic entropy change curves for different applied fields collapse onto a single curve for materials with second-order phase transition.

Keywords: Rare earth manganites, Ferromagnetic order, Magnetocaloric effect, Magnetic entropy, and Universal curve.

1. Introduction

Materials with simultaneous presence of more than one ferroic property (multiferroics) with a strong coupling between them have been the subject of tremendous research activity in recent years. Control of electric polarization by the application of magnetic field and inducing magnetic ordering by the application of electric field in these materials are expected to lead to next generation multifunctional devices for applications in information storage processes, spintronics, multiple-state memories, magnetoelectric sensors, etc. [1–4]. One typical example of multiferroic materials is hexagonal manganites $RMnO_3$ with space group $P6_3cm$, for elements at the rare-earth R site with a relatively small ionic radius, e.g., Ho, Er, Tm, Yb, Lu, Y, and Sc which exhibit a strong coupling between electric and magnetic dipoles [5–7]. In these hexagonal manganites, Mn ions form a natural two dimensional edge-sharing triangular network, which becomes magnetically frustrated with an antiferromagnetic nearest-neighbor interaction [8,9].

Among rare earth hexagonal manganites $YbMnO_3$ has been studied only occasionally. The crystal structure of $YbMnO_3$ comprises layers of corner-sharing MnO_5 trigonal bipyramids with two apical (O1, O2) oxygen atoms and a triangular base of nonequivalent O3 and O4 oxygen atoms. Yb atom occupies two crystallographic sites (in Wyckoff notations), 2a and 4b of space group $P6_3cm$. The Yb–O displacements give rise to a ferroelectric moment along the c -axis ($T_C = 990$ K), the Mn^{3+} moments order at the Neel temperature ($T_N = 85$ K) and below $T_C \sim 5$ K, the magnetic moments of the Yb^{3+} ions are completely ordered [10, 11]. Most of the studies in such multiferroic manganites focus on their magnetic and ferroelectric behavior, but less work has been undertaken on exploring their magnetocaloric effect (MCE) properties.

MCE describes the reversible change in temperature of a material under adiabatic condition produced by the magnetic entropy change ΔS_M due to the variation in applied

magnetic field [12,13]. The main aim in this field is to search for new materials that exhibit a large MCE and are capable of operating at different temperature ranges, depending on the intended applications. Large MCE close to room temperature would be useful for domestic and several technological applications while large MCE in the low-temperature region is important for specific technological applications such as space science and liquefaction of hydrogen in fuel industry [12,14]. The guidelines for the choice of an appropriate material are that it should have low heat capacity and exhibit a large entropy change at the ferromagnetic (FM) to paramagnetic (PM) transition or field-induced metamagnetic transition from antiferromagnetic (AFM) to FM states with a minimal hysteresis.

In the present report, effect of Sc substitution on structural, magnetic and magnetocaloric properties in the $\text{Yb}_{1-x}\text{Sc}_x\text{MnO}_3$ ($x = 0.1$ and 0.2) system is studied. In order to successfully use multiferroic materials in practical applications, the most important criterion is that the coupling between the ferroelectric and magnetic ordering should occur close to room temperature. Thus, it is necessary to enhance the low antiferromagnetic ordering T_N of YbMnO_3 through chemical doping. In our previous paper [10] on divalent Mg ion doped YbMnO_3 , it is shown that T_N increases marginally with doping. The increase in T_N can be explained on the basis of smaller cell volume (Mg has small ionic radii), which may lead to strong exchange interactions and therefore higher ordering temperatures. Hence, it is of significance to search for other effective dopants. Hexagonal ScMnO_3 exhibits an antiferromagnetic (AFM) transition at 139 K [15] and Sc^{3+} has small ionic radius compare to that of Yb^{3+} . The large field induced magnetization observed in $\text{Yb}_{1-x}\text{Sc}_x\text{MnO}_3$ has motivated us to investigate the magnetocaloric behavior in this system.

2. Experimental Details

Polycrystalline samples of $\text{Yb}_{1-x}\text{Sc}_x\text{MnO}_3$ ($x = 0.1$ and 0.2) were synthesized by the conventional solid state reaction method. High-purity (purity better than 99.9%) Yb_2O_3 ,

Sc₂O₃ and MnCO₃, powders are obtained from M/s Sigma-Aldrich. The precursors Yb₂O₃ and Sc₂O₃ powders are preheated at 500 K for 5 h to remove any absorbed moisture. Stoichiometric proportions of Yb₂O₃, Sc₂O₃ and MnCO₃ powders are thoroughly mixed, and then calcined in platinum crucibles at 1150 °C in air for 24 h with an intermediate grinding for homogenization. The calcined mixture is cold pressed into pellets at approximately 5×10⁷ Pa pressure and then sintered at 1350 °C in air for 20 hours. Finally, all samples are slowly cooled to room temperature for sufficient oxygenation. The phase purity of each sample is checked by powder x-ray diffraction (XRD) using a Bruker D8 Advance X-ray powder diffractometer operating with the Cu-Kα radiation. The magnetization measurements, performed in a Cryogenic Inc. (UK) make vibrating sample magnetometer operating at 20.4 Hz. The temperature dependence of magnetic moment was measured for zero-field cooled (ZFC) and field cooled (FC) conditions at a magnetic field of 1000 Oe. The magnetization isotherms in fields up to 10 T were measured, at different temperatures in the vicinity of low temperature ordering transition.

3. Results and Discussion

3.1. Structural characterization

The X-ray diffraction patterns and the Rietveld refinement of polycrystalline samples Yb_{1-x}Sc_xMnO₃ (x = 0.1 and 0.2) are shown in Fig. 1. Both samples are in single phase and the measured patterns can be indexed to the hexagonal phase with P6₃cm space group (JCPDS NO.38-1246) in agreement with a previous report [10]. Refined values of lattice parameters and discrepancy factors for Yb_{1-x}Sc_xMnO₃ (x = 0.1 and 0.2) are shown in Table 1 along with corresponding values for YbMnO₃. It is clearly seen that due to Sc substitution, the relative cell parameter c/a increases. Overall the cell volume decreases. The decrease in lattice constant *a* and cell volume is due to the smaller ionic radius of Sc³⁺ [Shannon radius = 0.87 Å for coordination number (CN) = 8] than Yb³⁺ (Shannon radius = 0.985 Å for CN = 8). As the

average *A*-site (i.e., Yb site) radius changes with Sc content, it is expected that the tolerance factor will also change.

Some selected bond distances and bond angles of $\text{Yb}_{1-x}\text{Sc}_x\text{MnO}_3$ ($x = 0.1$ & 0.2) as well as those of YbMnO_3 are given in Table 2. The value of *a* decreases in Sc doped sample when compared to that in YbMnO_3 sample. This change is ascribed to the decrease in the average *ab*-plane i.e., Mn-O3, Mn-O4 is on Sc doping. The Mn-O1 and Mn-O2 bond lengths are also decrease along the *c* axis on Sc doping. The average Mn-O distances in MnO_5 units are significantly shorter in the doped samples compared to pure YbMnO_3 . In the hexagonal phase the Mn^{3+} ion is fivefold coordinated, forming a trigonal bipyramid polyhedral environment. Polyhedral distortions Δ are calculated using the following formula [17],

$$\Delta = \frac{1}{N} \sum_{n=1}^N \left(\frac{d_n - \langle d \rangle}{\langle d \rangle} \right)^2 \quad (1)$$

Where *N* is the coordination number (*N* = 5), d_n is the individual distance between Mn and the n^{th} nearest oxygen neighbor, and $\langle d \rangle$ is the average distance value.

The distortion parameter is nearly constant with the Sc content in the hexagonal phase. In general, the Sc doping does not notably affect the structure of the MnO_5 polyhedron, in agreement with the weak changes of the trigonal bipyramidal crystal field, which is proved by the fact that the Mn^{3+} ions ($3d^4$) remain in the high spin state (*S*=2) throughout the whole doping range. The Mn-O bond lengths are in agreement with the sum of the ionic radii [15]. Moreover, in the YbO_7 polyhedron, the Yb-O distances are larger in $x = 0.1$ sample than in $x = 0.2$ sample, as expected due to the larger ionic radius of Yb^{3+} when compared to Sc^{3+} . Also, the average Yb-O distances are close to the sum of the ionic radii.

3.2. Magnetic behaviors

Fig. 2 shows the temperature dependence of the susceptibility $\chi = M/H$ of $\text{Yb}_{1-x}\text{Sc}_x\text{MnO}_3$ ($x = 0.1$ and 0.2) measured at a magnetic field $H=1000$ Oe. The susceptibility strongly increases with the decrease in the temperature at about 5 K. In the upper inset, we have shown zero field cooled (ZFC) and field cooled (FC) curves in the low-temperature region below 10 K. Near about 5.5 K both the curves show an anomaly with a sudden increase in magnetization with decreasing T . This abrupt change corresponds to the ferromagnetic (FM) ordering of Yb^{3+} moments at the $2a$ crystallographic sites through Yb-Yb interactions [18]. A second anomaly (a kink) is observed at 90 K for $x = 0.1$ and 94 K for $x= 0.2$, as shown in the lower inset of figure 2, which correspond to the AFM ordering of the Mn^{3+} moments and represent Neel temperatures (T_N) for these samples. Further, from the Rietveld refinement study it is observed that the average bond distance between the manganese and oxygen atoms decreases with increases in Sc content. This increases the covalence of Mn–O bonds and results stronger exchange interaction. It may be noted that lattice parameter a decreases with the Sc content and the magnetic interaction occurs in the a – b plane of the hexagonal manganites. Therefore, the increase in covalence of Mn–O accounts for both the increase in magnetic ordering temperature and the decrease in the lattice parameter a . The increase in T_N from 85 K for YbMnO_3 [16] to 94 K for $\text{Yb}_{0.8}\text{Sc}_{0.2}\text{MnO}_3$ sample also can be explained on the basis of smaller cell volume, which might lead to strong exchange interactions and therefore higher ordering temperatures.

Temperature variation of inverse magnetic susceptibility is plotted in fig.2 which shows that the Curie–Weiss (CW) law is well obeyed in temperature interval between 200 and 300 K in paramagnetic phase. It fits well to the Curie-Weiss law $\chi = C/(T-\theta_{\text{cw}})$. The values of paramagnetic Curie temperature (θ_{cw}) and effective magnetic moment (μ_{eff}) are calculated from this Curie-Weiss fit which are listed in Table 3. The negative Weiss temperature indicates presence of the antiferromagnetic interaction in these compounds. The

experimental effective magnetic moments of $\text{Yb}_{1-x}\text{Sc}_x\text{MnO}_3$ ($x = 0.1$ and 0.2) samples are obtained from the relation $\mu_{\text{eff}} = (7.99C)^{0.5}$, where C is the Curie–Weiss constant [10]. It is seen that the effective moment (μ_{eff}) decreases with increases in nonmagnetic Sc content. The experimental values of μ_{eff} are in reasonable agreement with the calculated values using the following formula: $\mu_{\text{eff}} = ((1-x)\mu_{\text{Yb}}^2 + \mu_{\text{Mn}}^2)^{1/2}$, where x is the Sc concentration while μ_{Yb} and μ_{Mn} are the effective magnetic moment of Yb^{3+} ($\mu_{\text{Yb}} = 4.53\mu_B$), and Mn^{3+} ($\mu_{\text{Mn}} = 4.9\mu_B$), respectively. The ratio $f = |\theta_{\text{CW}}/T_N|$, which is a measure of geometric frustration, is around 2.05. It is smaller for Sc doped samples when compared to that of YbMnO_3 , which indicates that the magnetic coupling between the Yb and the Mn moments in presence of Sc relieves the frustration effect as the magnitude of the magnetically coupling between Yb and Mn ions is the most important factors for the geometrical frustration.

The isothermal magnetization (M-H) curves of $\text{Yb}_{1-x}\text{Sc}_x\text{MnO}_3$ ($x = 0.1$ and 0.2) measured at 2.5 K are shown in Fig.3. Both the samples show a small magnetic hysteresis loops in low fields indicating a weak ferromagnetic (FM) behavior due to Yb^{3+} [18,20]. At 2.5 K, the ferromagnetic (FM) behavior is observed with corresponding coercivity (H_c) around 500 Oe. A change in Sc concentration slightly changes coercivity but retentivity decreases with increase in the Sc content as shown in the inset fig. 3. The isothermal magnetization (M-H) at 2.5 K also shows a noticeable sudden increase in magnetization around 30 kOe, similar results are observed in RMnO_3 in general and is attributed due to a magnetically induced phase transition where the Mn^{3+} ions ordering changes from AFM to FM along the c -axis while along the ab -plane the ordering remains unchanged to AFM [20-23]. Further, M does not saturate up to 100 kOe. As for $\text{Yb}_{0.9}\text{Sc}_{0.1}\text{MnO}_3$ and $\text{Yb}_{0.8}\text{Sc}_{0.2}\text{MnO}_3$, the magnetization at 100 kOe is $1.6\mu_B$ and $1.3\mu_B$, respectively. The magnetization of these samples decreases with increasing Sc concentration, which is nonmagnetic.

To explain the role of applied magnetic field on metamagnetic transition, the isothermal magnetization curves as a function of magnetic field for $\text{Yb}_{1-x}\text{Sc}_x\text{MnO}_3$ ($x = 0.1$ and 0.2) were measured in applied fields of up to 10 T in the temperature range of 2–40 K. Fig. 4 shows the typical isothermal magnetization curves of $\text{Yb}_{1-x}\text{Sc}_x\text{MnO}_3$ ($x = 0.1$ and 0.2), which upholds a field-induced metamagnetic transition [24]. The isotherms vary almost linearly in the low-field region and depending upon the temperature the slope changes at a critical field H_c without any indication of saturation. From these plots, below T_c , M increases slowly with H in the low field region the slope changes at a critical field H_c and then increases slowly with further increase of H .

To understand the nature of the metamagnetic phase transitions, we have transformed the $M(H)$ data into Arrott plots as shown in fig. 5[25]. Banerjee [26] has given an experimental criterion, which allows the determination of the nature of the magnetic transition (first or second order). It consists in observing the slope of the isotherms plots M^2 versus H/M . Applying a regular approach, the straight line was constructed simply by extrapolating the high magnetization parts of the curves for each studied temperature. The negative slope of the Arrott plot indicates a first order nature of the transition, while the positive slope implies a second order transition. It is seen from fig. 5 that the Arrott plots have positive slopes above and below T_c for $\text{Yb}_{1-x}\text{Sc}_x\text{MnO}_3$ ($x = 0.1$ and 0.2) samples in the complete M^2 ranges, indicating that the system exhibits a second order AFM to FM phase transition.

3.3. Magnetocaloric behaviors

In the isothermal process of magnetization, the MCE of the materials can be derived from Maxwell's thermodynamic relationship [27]:

$$\left(\frac{\partial M}{\partial T}\right)_H = \left(\frac{\partial S}{\partial H}\right)_T \quad (2)$$

The magnetic-entropy change ΔS_M , which results from the spin ordering (i.e. ferromagnetic ordering) and is induced by the variation of the applied magnetic field from 0 to H is given by

$$\Delta S_M(T, H) = \int_0^H \left(\frac{\partial M}{\partial T} \right)_H dH \quad (3)$$

For magnetization measured at discrete field and temperature intervals, the magnetic entropy change defined in Eq. (3) can be approximated by the equation (4) [28]:

$$\Delta S_M(T_{av})_{\Delta H} = \frac{\delta H}{2\delta T} \left(\delta M_1 + 2 \sum_{k=2}^{n-1} \delta M_k + \delta M_n \right) \quad (4),$$

with the uncertainty in $\Delta S_M(T_{av})_{\Delta H}$ as

$$\sigma |\Delta S_M(T_{av})_{\Delta H}| = \frac{1}{2|\delta T|} \left\{ \begin{array}{l} \left| \delta H \left(\sigma M_1 + 2 \sum_{k=2}^{n-1} \sigma M_k + \sigma M_n \right) \right| \\ \left| \delta M_1 | \sigma H_1 + 2 \sum_{k=2}^{n-1} (|\delta M_k | \sigma H_k) + |\delta M_n | \sigma H_n \right| \\ + 2 |\Delta S_M(T_{av})_{\Delta H}| \times (\sigma T_u + \sigma T_l) \end{array} \right\}$$

where, $\delta T = T_u - T_l$ is the temperature difference between the two isotherms measured at T_u and T_l with the magnetic field varying from H_l to H_n in constant steps of δH . $\delta M_k = M(T_u)_k - M(T_l)_k$ is the difference in the magnetization at T_u and T_l for each magnetic field H_k . For the calculation of relative error in the entropy change, following [28], the accuracy of magnetization measurements are taken as 0.5% and the accuracy of the magnetic field as 0.1%. The manufacturer quoted temperature stability of 0.25% is used as the error for temperatures. In general, the relative error in the calculated entropy change is 10-20% except at very high fields and low temperatures ($H \sim 10$ T, $T < 4$ K).

The magnetic entropy changes, $-\Delta S_M$ of $\text{Yb}_{1-x}\text{Sc}_x\text{MnO}_3$ ($x = 0.1$ and 0.2) samples, associated with the magnetic field variation (1 to 10 T) were calculated using Eq. (4) and the data for selected fields are displayed in fig. 6. These curves present a characteristic shape with a broad

maximum in the vicinity of the FM transition of Yb moment. The magnitude of the peak increases with increasing the value of ΔH for each composition and the position of the maximum shifts from 5 to 7.5 K when the magnetic field change increases from 1 to 10 T. The maximum entropy change, $-\Delta S_M^{\max}$, corresponding to a magnetic field variation of 10 T is found to be 2.46 ± 0.40 J/mole-K and 1.87 ± 0.31 J/mole-K for $x = 0.1$ and 0.2 , respectively. The magnitude of $|\Delta S_M^{\max}|$ increases linearly with increasing magnetic field. The field induced metamagnetic transition contributes to the enhancement of ΔS_M [29]. These values are in agreement with the reported values in the literature which are ~ 2.3 J mole⁻¹K⁻¹ for $H = 8$ T for single crystal YbMnO₃ [24]. For comparison, we list in data of various magnetic materials in Table 3 which could be used as magnetic refrigerants.

When comparing different magneto-caloric materials, it is useful to calculate their relative cooling power (RCP) based on the magnetic entropy change. The relative cooling power is evaluated by considering the magnitude of ΔS_M and its full width at half-maximum δT_{FWHM} was expressed as follows [30]:

$$RCP = |\Delta S_M^{\max}| \times |\delta T_{FWHM}| \quad (5),$$

It is a measure of the quantity of heat transferred by the magnetic refrigerant between hot and cold sinks. The results of these calculations are shown in Fig. 7(b). We estimate a relative error of 15-30 % for the RCP values (as field increases from low: 1 T to high: 10 T) considering the relative error of 10-20% in the value of $|\Delta S_M^{\max}|$ and considering a 5-10% error in assigning the δT_{FWHM} values. The RCP values show increase with increasing field for both compounds. RCP values are 38.5 ± 9 J/mol, and 30.1 ± 8 J/mol with $\Delta H = 10$ T for samples with $x = 0.1$ and 0.2 , respectively. These values are higher than those for single crystal YbMnO₃ (RCP = 26 J/mole with $\Delta H = 8$ T) [24]. Thus, RCP values of these compounds indicate that these are potential candidates for applications at low temperatures.

Figure 7(a) shows the dependence of the magnetic entropy change on the parameter $h^{2/3}$ [31,32] where h is the reduced field just around T_c and is given by $\left[h = \frac{(\mu_B H)}{(K_B T_C)} \right]$. The mean-field theory predicts that in the vicinity of second-order phase transitions, $\Delta S_M^{\max} = -kM_s(0)h^{2/3} - S(0,0)$, here k is a constant, $M_s(0)$ is the saturation magnetization at low temperatures and $S(0, 0)$ is the reference parameter, which may not be equal to zero [33,34]. Fig.7(a) shows the linear dependence of ΔS_M^{\max} versus $h^{2/3}$ which implies the second order transition for $\text{Yb}_{1-x}\text{Sc}_x\text{MnO}_3$ ($x = 0.1$ and 0.2). The fact that ΔS_M^{\max} is estimated around T_C and in fields larger than the critical field required for the metamagnetic transition, the conclusion about the second order transition is justified.

3.4. Universal curve

The construction of the phenomenological universal curve is based on the collapse of the $\Delta S_M(T, H)$ points into one single point in the new curve corresponding to equivalent states of the system. Those equivalent states have the same height, in the $(-\Delta S_M / \Delta S_M^{\max})$ curves. The collapse of the normalized entropy change curves can be then obtained by defining a new variable for the temperature axis, θ , given by the expression

$$\theta = -\frac{T-T_C}{T_{r1}-T_C}, \quad T \leq T_C \quad (6(a))$$

$$\theta = \frac{T-T_C}{T_{r2}-T_C}, \quad T > T_C \quad (6(b))$$

where T_{r1} and T_{r2} are the temperature of the two reference points that, for the present study, have been selected as those corresponding to $\Delta S_M(T_{r1,2}) = 1/2 \Delta S_M^{\max}$ [35]. Fig.8 shows the dependence of ΔS^* ($-\Delta S_M / \Delta S_M^{\max}$) for $\text{Yb}_{1-x}\text{Sc}_x\text{MnO}_3$ ($x = 0.1$ and 0.2) for typical field changes. It can be clearly seen that the experimental points of the samples distribute on one universal curve of the magnetic entropy change (ranging from 4 T up to 10 T). The universal curve can be well fitted by a Lorentz function [35]

$$\Delta S^* = \frac{a}{b + (\theta - c)^2}, \quad (7)$$

where a , b , and c are the free parameters. A fit to this relation gives $a = 1.0246$, $b = 1.01$, and $c = -0.05$. According to Eq. 7, only the position and magnitude of the peak, namely, T_C and ΔS_M^{\max} , and two reference temperatures T_{r1} and T_{r2} , are needed to characterize the entropy change, where $T_{r1} < T_C$ and $T_{r2} > T_C$. That is to say, to translate S into the “real” $\Delta S_M(T)$, one needs only these values that are determined by the properties of the materials. Thus, incomplete $\Delta S_M(T)$ curves, which are experimentally determined from a small temperature span in the vicinity of T_C for the isothermal magnetization measurements, can be easily transformed into the complete curves, which is a helpful tool for the evaluation of material properties such as the refrigerant capacity RC.

3.5. Conclusion

In conclusion, we report detailed investigations of structural, magnetic and magnetocaloric properties of $\text{Yb}_{1-x}\text{Sc}_x\text{MnO}_3$ ($x = 0.1$ and 0.2) revealing the effect of Sc doping in YbMnO_3 on the structure (*bond length, bond angles, unit cell volume, tolerance factor, distortion of MnO_5 polyhedra*) and magnetism (increase in T_N , change in frustration parameter, f). From analysis of experimental data, we deduced RCP of $\text{Yb}_{1-x}\text{Sc}_x\text{MnO}_3$, which are found to be 38.5 ± 9 J/mol, and 30.1 ± 8 J/mol with $\Delta H = 10$ T for $x = 0.1$ and 0.2 respectively. Thus, multiferroic manganites seem to be potential materials for magnetic refrigeration in the low temperature region. The behavior of ΔS_M^{\max} vs $h^{2/3}$ curve confirm that present materials exhibit a second order transition. The phenomenological construction of the universal curve for the studied $\text{Yb}_{1-x}\text{Sc}_x\text{MnO}_3$ ($x = 0.1$ and 0.2) with a Lorentz function is a helpful tool for the evaluation of material properties such as the refrigerant capacity RC.

Acknowledgement

This work has been supported by UGC-DAE Consortium for Scientific Research, Mumbai Centre, India in the form of a collaborative research scheme (CRS) through project number CRS-M-199. BSB acknowledges UGC-DAE CSR, Mumbai Centre for project fellowship. AKB is thankful to the National Academy of Sciences, India for their support to this work through Senior Scientist Platinum Jubilee Fellowship Scheme. Thanks to Dr. K Gireesan, IGCAR, Kalpakkam for providing help in part of this work and also thanks to Dr.B. Koteswara Rao, DST-INSPIRE Faculty for fruitful discussions.

Table 1. Refined crystallographic parameters and reliability factors of Rietveld refinement for $\text{Yb}_{1-x}\text{Sc}_x\text{MnO}_3$ ($x = 0.1$ & 0.2) samples at room temperature.

$\text{Yb}_{1-x}\text{Sc}_x\text{MnO}_3$	$x = 0.1$	$x = 0.2$	Reported values for YbMnO_3 [10,16].
a (Å)	6.0577(4)	6.046(4)	6.0671 (4)
c (Å)	11.362(4)	11.3575(4)	11.3519 (4)
V (Å ³)	361.07(2)	359.542(2)	361.886 (2)
c/a	1.8756	1.8785	1.8710
χ^2	4.12	5.97	-
$R_p(\%)$	6.55	6.67	5.06
$R_{wp}(\%)$	8.28	8.86	6.82
$R_B(\%)$	4.05	5.34	4.50
t (Å)	0.846	0.842	0.850

t is the tolerance factor, given as: $t = ((r_{\text{Yb+Sc}} + r_o) / \sqrt{2}(r_{\text{Mn}} + r_o))$.

Table.2. Main bond distances (Å) and angles for MnO₅ polyhedra in Yb_{1-x}Sc_xMnO₃ (x = 0.1 and 0.2)

Parameter	x = 0.1	x = 0.2	Reported values for YbMnO ₃ [7].
Mn-O1	1.8442	1.8434	1.8532
Mn-O2	1.8019	1.8011	1.8366
<Mn-O1, O2>	1.823	1.822	1.845
Mn-O3	1.9104	1.9067	1.9033
Mn-O4	2.0931	2.0891	2.1017
<Mn-O3, O4>	2.002	1.9979	2.0025
<Mn-O>	1.9125	1.9099	1.9237
∑Radii	2.00	2.00	2.00
Yb1-O1(X3)	2.3781	2.3745	-
Yb1-O2(X3)	2.4719	2.4676	-
Yb1-O3	2.3251	2.3242	-
Yb2-O1(X3)	2.1853	2.1816	-
Yb2-O2(X3)	2.2765	2.2733	-
Yb2-O4	2.4439	2.4729	-
<Yb-O>	2.3468	2.349	-
∑Radii	2.405	2.405	-
Mn-O3-Mn (°)	118.644(3)	118.64(6)	119.5 (7)
Mn-O4-Mn (°)	119.04(3)	119.038(5)	118.6 (2)
$\Delta(10^{-4})$	27	26.5	24.14

Δ is the distortion of MnO₅ polyhedra.

Table.3.Values of magnetic parameter of $\text{Yb}_{1-x}\text{Sc}_x\text{MnO}_3$ ($x = 0.1$ and 0.2). Also listed are magnetocaloric effect (MCE) parameters: ΔS_M^{\max} and RCP with reported values.

	From Curie-Wiess fit					MCE			
	$\mu_{\text{eff}}^{\text{Exp}}(\mu_B)$	$\mu_{\text{eff}}^{\text{Theor}}(\mu_B)$	$\theta_{\text{CW}}(\text{K})$	$T_N(\text{K})$	$f = \theta_{\text{CW}}/T_N $	$\Delta H(\text{T})$	$\Delta S_M^{\max}(\text{Jmol}^{-1} \text{K}^{-1})$	RCP (J mol^{-1})	
x = 0.1	6.1	6.5	-182	90	2.02	5	1.32	13.8	
						10	2.43	38.5	
x = 0.2	5.6	6.3	-193	94	2.05	5	1.01	10.2	
						10	1.88	30.1	
Reported values for YbMnO_3									
Ref 10	5.91	6.68	-219	85	2.57	8	2.3	26	Ref 20
Ref 18	6.1	6.68	-220	85	2.58	10	2	26	Ref 16
Ref 19	6.40	6.68	-166	82	2.02	-	-	-	

References.

- [1] M. Fiebig, J. Phys.D., 2005,**38**, R123–R152.
- [2] W. Prellier, M.P. Singh, P. Murugavel, J. Phys. Condens. Matter., 2005,**17**,R803–R832.
- [3] N.A. Spaldin, M. Fiebig, Science., 2005,**309** , 391–392.
- [4] X. Qi, J. Dho, R. Tomov, M.G. Blamire, J.L. MacManus-Driscoll, Appl.Phys.Lett., 2005,**86**, 062903(1)–062903(3).
- [5] Z.J. Huang, Y. Cao, Y.Y. Sun, Y.Y. Xue, C.W. Chu, Phys. Rev. B., 1997,**56**, 2623-2626.
- [6] T. Katsufuji, S. Mori, M. Masaki, Y. Moritomo, N. Yamamoto, H. Takagi, Phys.Rev.B., 2001,**64**, 104419(1)–104419(6).
- [7] M. Fiebig, Th. Lottermoser, D. Frohlich, A.V. Goltsev, R.V. Pisarev, Nature .,

2002,419, 818–820.

[8] T. Katsufuji, M. Masaki, A. Machida, M. Moritomo, K. Kato, E. Nishibori, M. Takata, M. Sakata, K. Ohoyama, K. Kitazawa, and H. Takagi, *Phys. Rev. B.*, 2002, **66**, 134434.

[9]. P. Schiffer and A. P. Ramirez, *Condens. Matter Phys.*, 1996, **18**, 21.

[10]. B. Sattibabu, A. K. Bhatnagar, Sudhindra Rayaprol, D. Mohan, D. Das, M. Sundararaman, V. Siruguri, *Physica B.*, 2014, **448**, 210.

[11]. Th. Lonkai, D. G. Tomuta, U. Amann, J. Ihringer, R. W. A. Hendrikx, D. M. Toëbbens, J. A. Mydosh, *Phys. Rev. Lett.*, 2004, **69**, 134108.

[12]. K. A. Gschneidner Jr., V. K. Pecharsky, and A. O. Tsokol, *Rep. Prog. Phys.*, 2005, **68**, 1479 and references therein.

[13]. A. M. Tishin in *Handbook of Magnetic Materials*, edited by K. H. Buschow (Elsevier Science B.V., New York) 1999, **12** 395.

[14]. V. Provenzano, J. Li, T. King, E. Canavan, P. Shirron, M. DiPirro, and R. D. Shull, *J. Magn. Magn. Mater.*, 2003, **266**, 185.

[15]. A. Muñoz, J. A. Alonso, M. J. Martínez-Lope, M. T. Casañis, and J. L. Martínez and M. T. Fernández-Díaz *Phys. Rev. B.*, 2000, **62**, 9498.

[16]. B. Sattibabu, A. K. Bhatnagar, S. S. Samatham, D. Singh, S. Rayaprol, D. Das, V. Siruguri, and V. Ganesan, *J. Alloys and Compounds.*, 2015, **644**, 830–835.

[17] Rodríguez-Carvajal, J., Hennion, M., Moussa, F. & Moudden, A. H. *Phys. Rev. B.*, 1998, **57**, R3189–R3192.

[18]. X. Fabreges, I. Mirebeau, P. Bonville, S. Petit, G. Lebras-Jasmin, A. Forget, G. Andre, and S. Pailhes, *Phys. Rev. B.*, 2008, **78**, 214422.

- [19]. S.L. Samal , T. Magdaleno , K.V. Ramanujachary , S.E. Lofland , A.K. Ganguli, Journal of Solid State Chemistry., 2010,**183**, 643–648.
- [20]. H. Sugie, N. Iwata, K. Kohn, J. Phys. Soc. Jpn., 2002,**71**, 1558
- [21].M. Fiebig, C. Degenhardt, R. V. Pisarev, Phys. Rev. Lett. ,2002, **88**, 027203.
- [22].M. Fiebig , Th. Lottermoser, R. V. Pisarev J. Appl. Phys., 2003,**93**,8194.
- [23].N. Abramov, S. Lofland, and Ya. Mukovskii, phys. status solidi B, 2012,**1-3**,48318.
- [24] A. Midya, S. N. Das, P. Mandal, S. Pandya and V. Ganesan, Phys. Rev. B.,20011,**84**, 235127.
- [25] A. Arrott and J. Noakes, Phys. Rev. Lett. ,1967, **19**, 786.
- [26] S. K. Banerjee, Phys. Lett. ,1964,**12**, 16.
- [27] A.H. Morrish, The Physical Principles of Magnetism Wiley, New York, 1965(Chapter3).
- [28] V.V. Pecharsky and K.A. Gschneidner, J. Appl. Phys., 1999,**86**,565.
- [29] A. Midya, P. Mandal,S. Das, S. Banerjee, L. S. Sharath Chandra, V. Ganesan and S.Roy Barman,Appl. Phys. Lett., 2010, **96**, 142514.
- [30] K.A. Gschneidner, V.K. Pecharsky, Annu. Rev. Mater. Sci., 2000,**30**, 387.
- [31] Wang J L, Campbell S J, Zeng R, Poh C K , Dou S X J. Appl. Phys.,2009,**105**,07A909.
- [32] Oesterreicher H and Parker F T J. Appl. Phys.,1984,**55**,4334.
- [33] V. Franco, A. Conde, V. K. Pecharsky and K. A. Gschneidner, EPL., 2007, **79**, 47009.
- [34] N. Zaidi,S. Mnefgui, J. Dhahriaand E. K. Hlil, RSC Adv., 2015, **5**, 31901.
- [35] Q. Y. Dong, H. W. Zhang,J. R. Sun, B. G. Shen, and V. Franco, J. Appl. Phys., 2008,**104**,116101.

Figure captions:

Fig.1. Rietveld refinement of room temperature XRD pattern of $\text{Yb}_{1-x}\text{Sc}_x\text{MnO}_3$ ($x = 0.1$ and 0.2) samples indexed in space group $P6_3cm$.

Fig.2. Temperature dependence of $1/\chi$ with Curie-Weiss fit and χ ($H = 1000$ Oe) of $\text{Yb}_{1-x}\text{Sc}_x\text{MnO}_3$ ($x = 0.1$ and 0.2): Upper inset: ZFC and FC curves of T near the FM transition of Yb^{3+} . Lower inset: ZFC and FC curves of T near the AFM transition of Mn^{3+} .

Fig.3. The hysteresis loops of $\text{Yb}_{1-x}\text{Sc}_x\text{MnO}_3$ ($x = 0.1$ and 0.2). Insert shows up to 1 tesla.

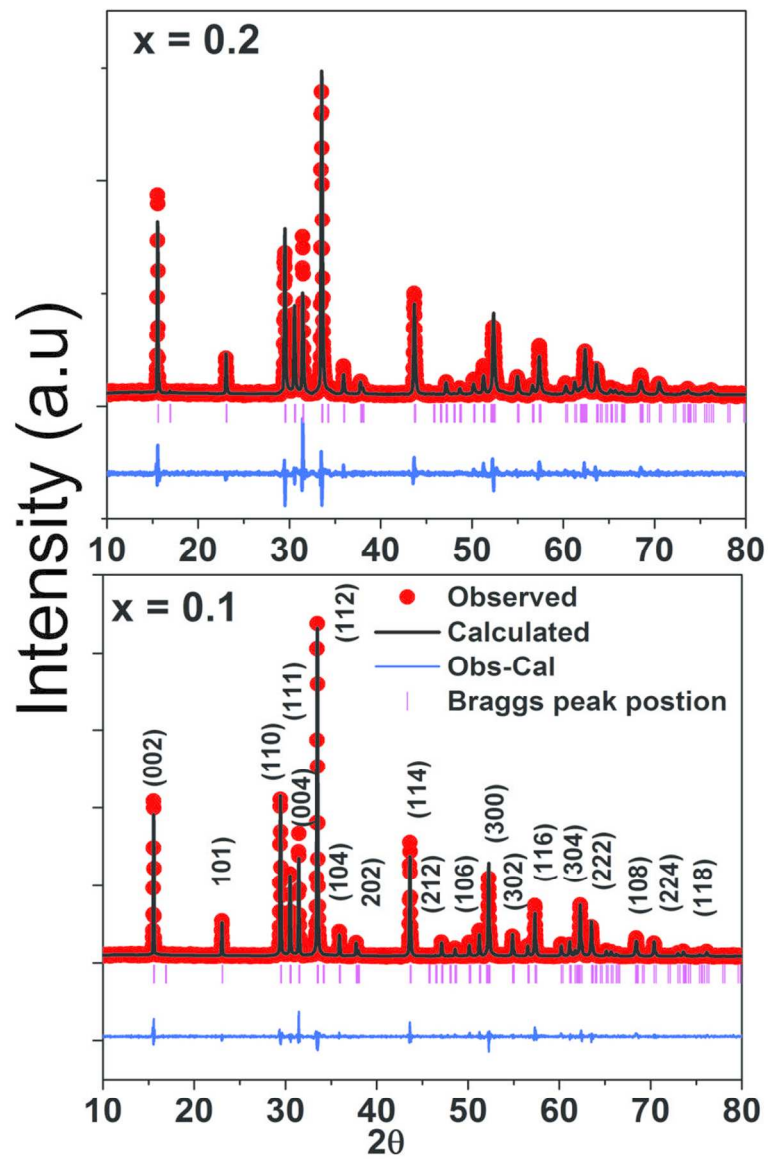
Fig.4. Field dependence of isothermal magnetization for $\text{Yb}_{1-x}\text{Sc}_x\text{MnO}_3$ ($x = 0.1$ and 0.2) at some selective temperatures.

Fig.5. The Arrott plots of M^2 vs. H/M at various temperatures for $\text{Yb}_{1-x}\text{Sc}_x\text{MnO}_3$ ($x = 0.1$ and 0.2) samples.

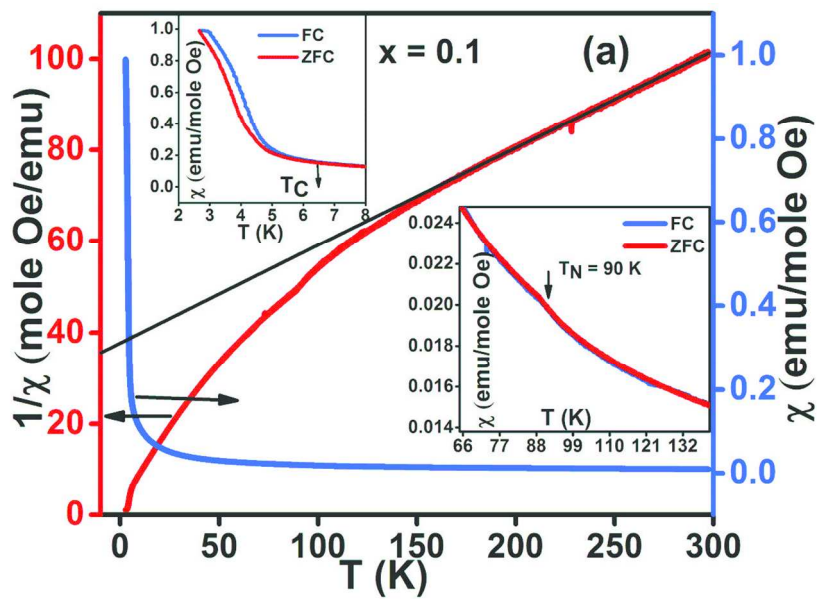
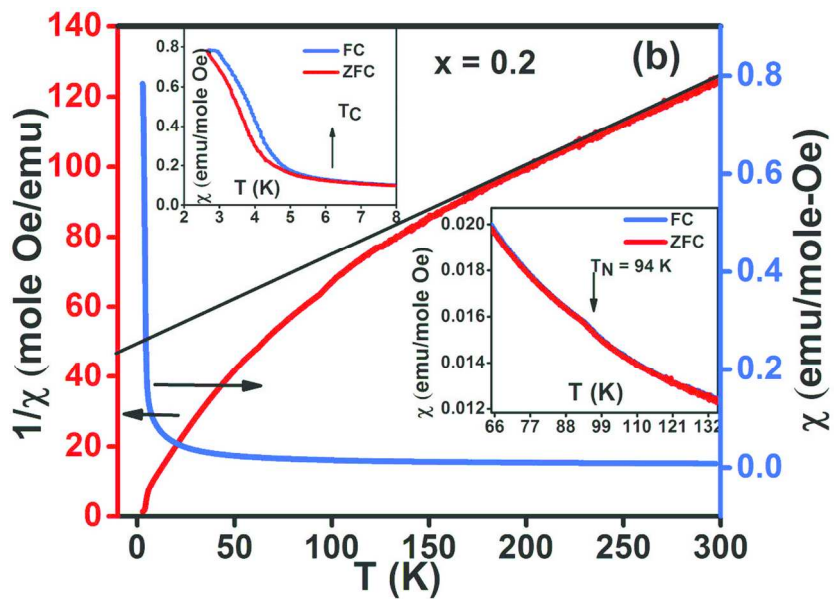
Fig.6. Temperature variation of magnetic entropy change for selected field change for $\text{Yb}_{1-x}\text{Sc}_x\text{MnO}_3$ ($x = 0.1$ and 0.2) samples.

Fig.7.(a) Temperature dependence of magnetic entropy change ΔS_M^{\max} versus $h^{2/3}$ (b) Relative cooling power as a function of field for $\text{Yb}_{1-x}\text{Sc}_x\text{MnO}_3$ ($x = 0.1$ and 0.2) samples.

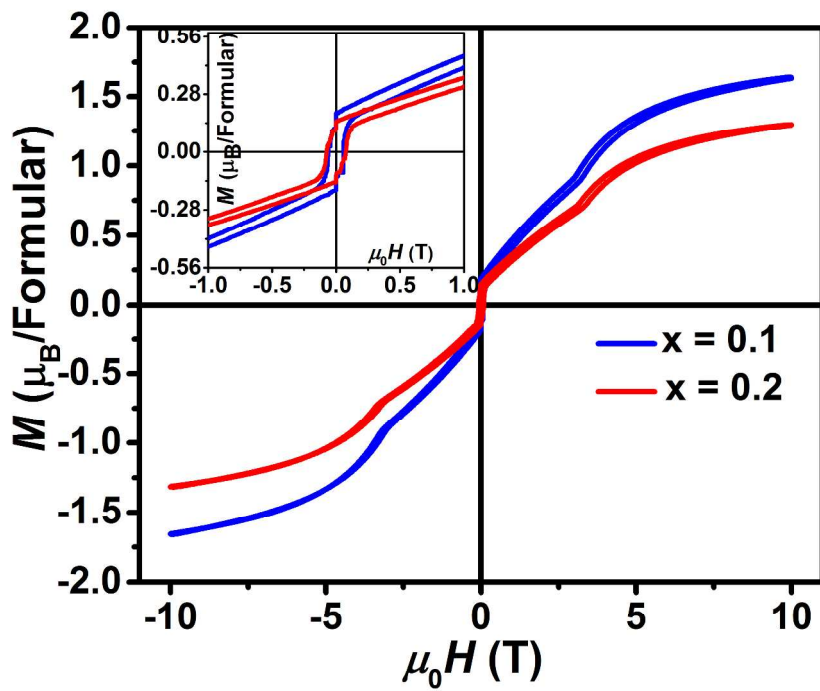
Fig.8. The universal curve behavior of the curves as a function of the rescaled temperature for different magnetic field for $\text{Yb}_{1-x}\text{Sc}_x\text{MnO}_3$ ($x = 0.1$ and 0.2).



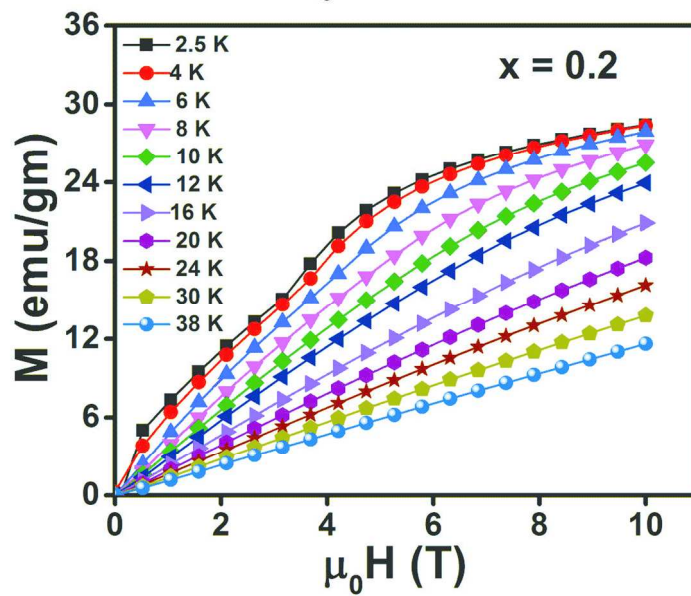
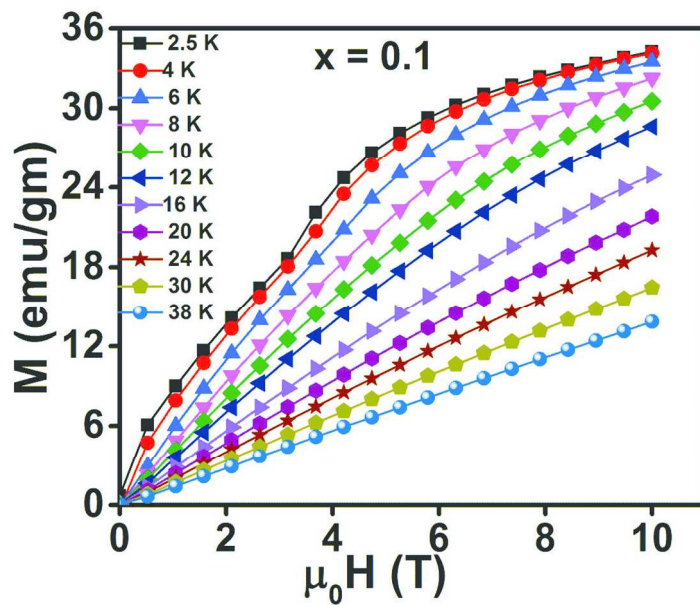
101x127mm (300 x 300 DPI)



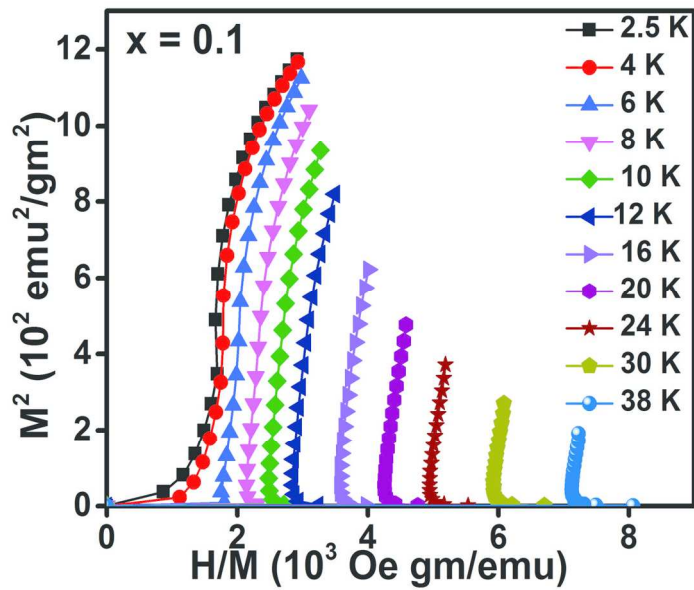
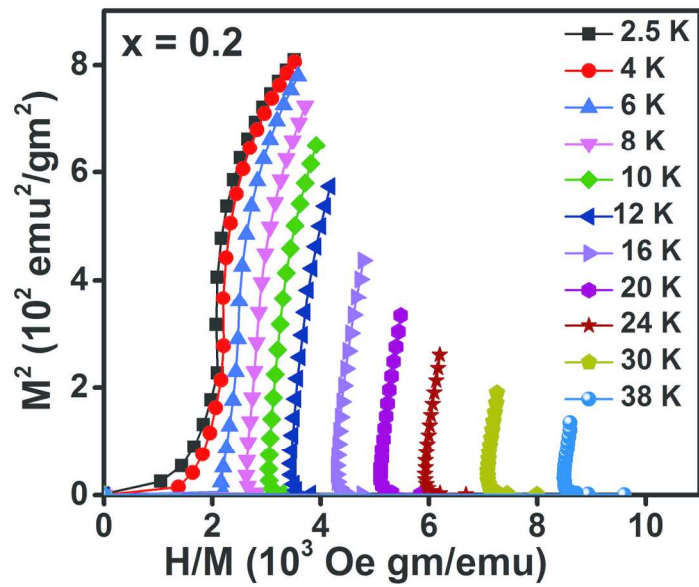
104x151mm (300 x 300 DPI)



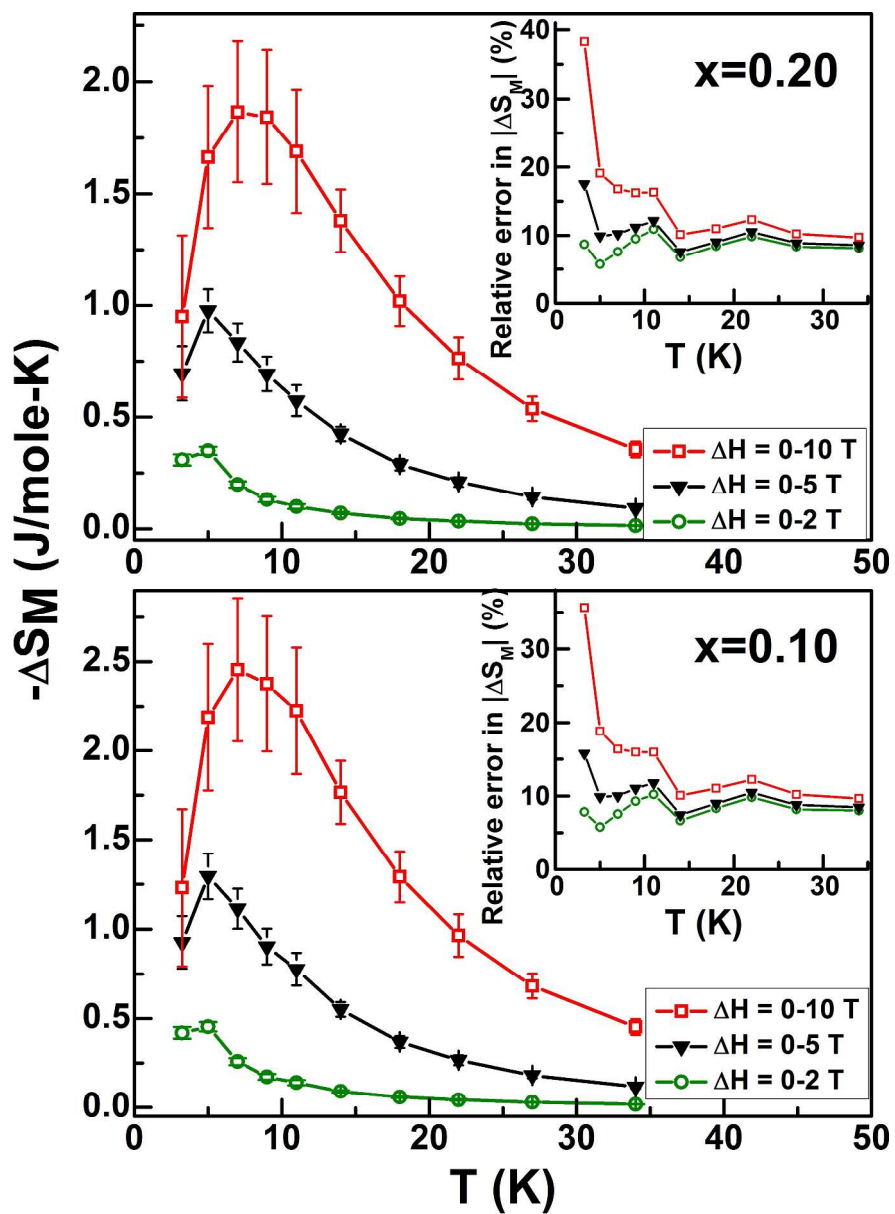
279x215mm (300 x 300 DPI)



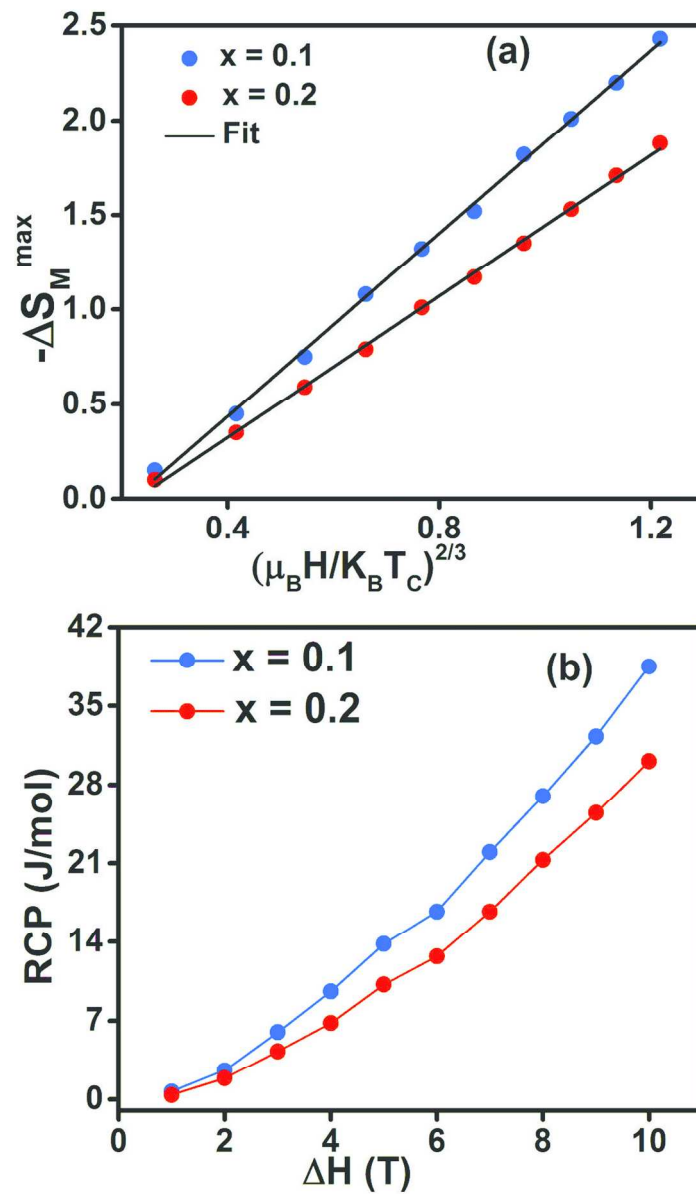
92x156mm (300 x 300 DPI)



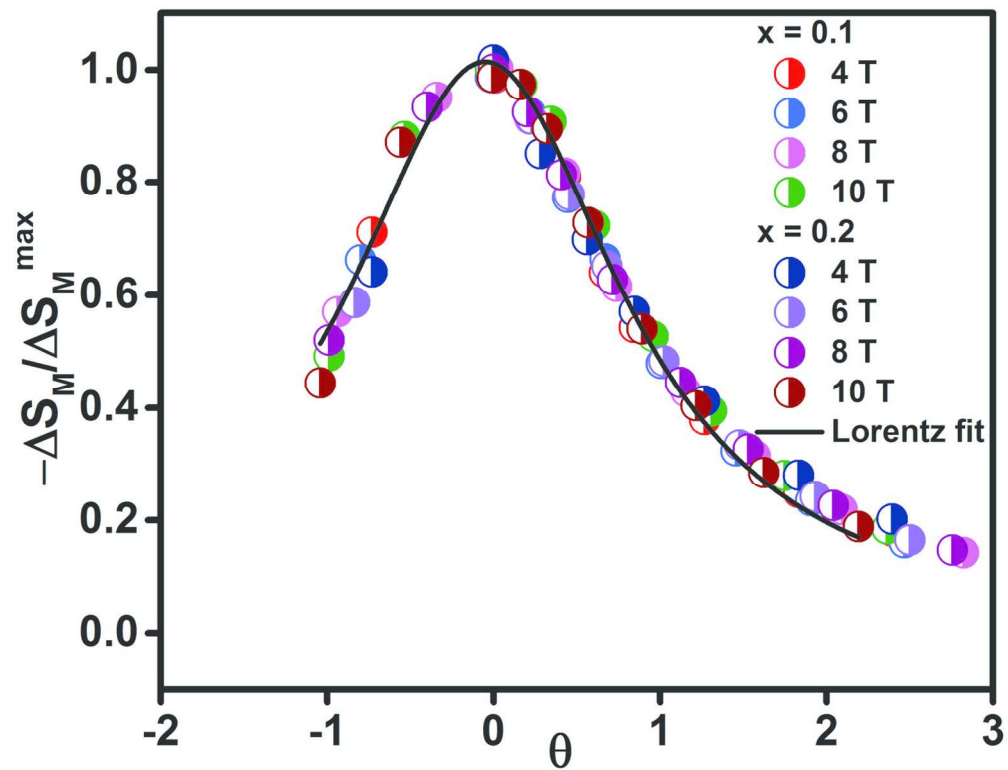
112x192mm (300 x 300 DPI)



284x390mm (299 x 299 DPI)



93x157mm (300 x 300 DPI)



137x106mm (300 x 300 DPI)